Size Distribution Dynamics in a Salting Out Crystallizer

D. C. MURRAY and M. A. LARSON

Iowa State University of Science and Technology, Ames, Iowa

A laboratory continuous mixed suspension salting out crystallizer was designed and constructed to test the dynamic crystallization model proposed by Randolph and Larson. The model relates the crystal size distribution to nucleation and growth kinetics and operating conditions. The ammonium alum-ethanol-water system was selected because of its ease of operation and control.

The results of this work were in agreement with the steady state model. Under the conditions of these experiments, it was found that the nucleation rate dN^o/dt was related to the growth rate r by $dN^o/dt = k_1 r^2$. The crystallizer was also operated under unsteady state conditions which resulted from variations in the production rate. The theoretical model with experimentally determined parameters was simulated on an analog computer and solved for production rate changes. The results indicated that the model was in agreement with the dynamic data for production rate upsets.

Much theoretical work has been done in the area of continuous mixed suspension, mixed product removal crystallization (*1, 5, 6, 8*) in recent years. Most of these studies used a probability density function called *the population density of the crystal distribution* as the characterizing variable. Theoretical agreement between authors is found for a steady state model of the size distribution. This steady state model is written as

$$n_o = n_o^o \exp\left(-L/r_o T_o\right) \qquad (1)$$

It has been found that this equation is in agreement with data taken from small experimental as well as large commercial crystallizers (*1, 6*).

An extensive theoretical study of unsteady state crystallization was carried out by Randolph and Larson (*6*). They derived from an unsteady state crystal numbers balance the following equation:

$$\frac{\partial n}{\partial t} = -r\frac{\partial n}{\partial L} - \frac{n}{T} \qquad (2)$$

The constraints and boundary conditions required for this equation are continuous operation, no seeding, perfectly mixed suspension, and mixed product removal, and an important assumption was the applicability of McCabe's ΔL law (*3*). This relationship presents an important milestone in the field of crystallization in that its solution provides information which may be used to operate and control continuous crystallizers. Equation (1) is the steady state solution to Equation (2).

There has been no published experimental unsteady state data which may be used to test the applicability of this equation. It was the purpose of this study to develop a laboratory procedure to obtain experimental unsteady state data to check the validity of Equation (2) for upsets in the production rate of the system. The response of the moments of the distribution described by Equation (2) to upsets in production rate was obtained by analog computer solution.

A continuous, mixed suspension, mixed product removal, salting out crystallizer was constructed which satisfied the constraints and assumptions incorporated in the development of Equation (2). Several crystallization systems were tested before one was found which yielded firm, regular crystals with a rapid growth rate. The system of ammonium alum-water-ethanol was found to fit these requirements. It formed firm, regular octahedral crystals with a growth rate such that 20-mesh crystals are formed in a period of thirty minutes.

The generation of supersaturation by addition of a third component was selected because of the many advantages in operation and control. Auxiliary equipment for heating, cooling, and vacuum generation was not needed as is necessary with evaporative or cooling types of crystallizers. The use of nonsaturated feed streams eliminated problems of feed-line plugging during operation. Insulation of the crystallizer was not necessary; therefore, a transparent vessel could be used enabling visual observation of the crystal suspension during operation. The maintenance of a constant crystal suspension during an upset in production rate did not require the simultaneous changing of heat input or removal. The above mentioned advantages are especially important when a very small crystallizer is used.

The particular system used, alum-water-ethanol, provided a rapid growth rate, a constant shape factor for all sized crystals, and a satisfactory density relationship between crystals and suspension. The specific gravity of the crystals and a typical suspension were 1.64 and 1.02, respectively. These properties permitted a very close approach to a perfectly mixed suspension.

EXPERIMENTAL

The crystallizer used for this work was a 5½-liter Plexiglas cylindrical vessel equipped with a propeller type agitator and a draft tube (*2*). Figure 1 shows the critical dimensions of the crystallizer assembly. The draft tube was supported on three legs which also acted as baffles. The two feed streams were added to the suspension at its surface from the external feed system.

The external flow system for the two feed streams is shown in Figure 2. The alum storage tanks were 55-gal. stainless steel drums, and the ethanol storage tank was a 5-gal. polyethylene bottle. All of the feed lines were ⅜-in. stainless steel tubing and contained filters to remove nonsoluble contaminants. Calibrated rotameters were used to control the flow of each stream. An automatic level controller was used to operate a product removal pump. Product removal was rapid and intermittent in order to give nonclassified product removal.

Samples of the suspension in the crystallizer were removed through a second suction tube placed midway in the annular

D. C. Murray is with Esso Research and Engineering Company, Baytown, Texas.

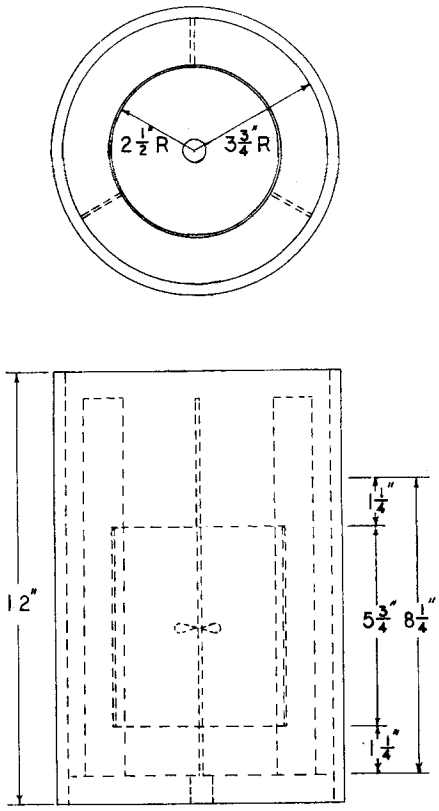

Fig. 1. Crystallization vessel.

channel. The samples were screened by suction through a 300-mesh screen.

Screen analyses were made with calibrated U. S. Standard 3-in. screens. The screens used were the following U. S. Standard mesh sizes: 16, 18, 20, 25, 35, 40, 50, 70, 100, 140, and 200. Because of the symmetry of the crystals, reproducible screen analyses were easily achieved.

To initiate an experimental run, the crystallizer was charged with the proper ratio of alum solution to alcohol, and the agitator and liquid level controller were turned on. The two feed streams were started and set at their proper flow rates. The flows were then maintained or changed depending on the type of run which was to be made. For the production rate step runs, the two incoming flows were simply changed at the proper time.

The samples of the crystal suspension taken through the submerged sampling tube varied from 500 to 700 ml. depending on the density of the suspension at the time of sampling. The suspension was separated by suction filtering through a 300-mesh screen in a funnel. The crystals were washed several times with acetone, taking care that as much liquor as possible was removed before the introduction of acetone. The crystals were then air dried by continuing the suction. When the crystals were dry, they were placed in a nest of calibrated U. S. Standard 3-in. screens and subjected to 10 min. of shaking. Each size fraction was separated and weighed. Samples were taken every two residence times during normal operation. Immediately after a step change in operation, however, they were taken more frequently to obtain a close measure of the transient results.

RESULTS

Treatment of Data

The crystal distributions obtained had a size range from 0.081 to 1.1 mm. and were divided by screen analyses into twelve size fractions. In order to represent the size distribution in terms of population density, the distribution was converted from weight fraction obtained from the screen analyses in the following manner:

1. The arithmetic average diameter of each size fraction was determined.
2. The total weight of crystals of a given size fraction was then divided by the crystal density, the cube of the average diameter, and a volumetric shape factor. This gave the number of crystals in the size fraction.
3. The number of crystals in each fraction was then divided by the width of the size range of the fraction. This gave the population density of crystals in the size fraction.

The actual calculation was performed by first making a cumulative weight percent plot. The abscissa of this curve was broken into twenty equal segments of 0.05 mm. width. The incremental value of the cumulative weight percent was read for each segment of the abscissa. The population density for each segment was then calculated by

$$n = \frac{\rho_s V}{\rho} \frac{\Delta m}{K_v \bar{L}^3 \Delta L} \tag{3}$$

The data thus treated are plotted in Figures 3 and 5 for the steady state size distribution and unsteady state, respectively. The data in tabular form are on file at the Chemical Engineering Department, Iowa State University, Ames, Iowa.

The total number of crystals was obtained by numerically integrating the above data to give

$$N_T = J_o = \int_o^\infty n dL \tag{4}$$

The total length, area, and mass obtained by numerically performing the following integrations:

$$L_T = J_1 = \int_o^\infty nL dL \tag{5}$$

$$A_T = J_2 = K_a \int_o^\infty nL^2 dL \tag{6}$$

$$M_T = J_3 = K_v \int_o^\infty nL^3 dL \tag{7}$$

Steady State

As is indicated by Equation (1), the steady state plot of log of population density vs. crystal size should give

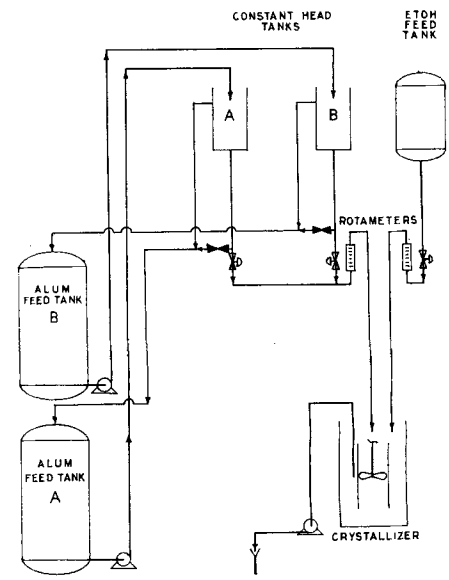

Fig. 2. Flow diagram of crystallization system.

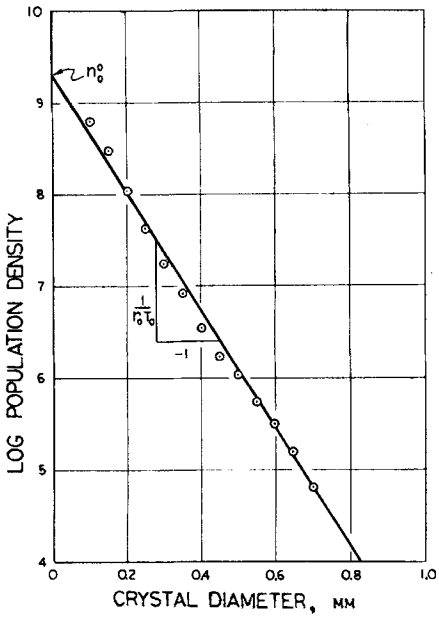

Fig. 3. Plot of log steady population density vs. crystal diameter: 15-min. residence time, 5/1 ratio of alum solution to ethanol, 10 g./100 ml. water alum solution concentration, 5.5-liter vessel.

a straight line with a slope proportional to $-1/r_o T_o$ and an intercept of log of nuclei population density. Figure 3 shows this steady state plot for a residence time of 15 min. The alum solution concentration was 10 g./100 ml. water, and the ratio of alum solution to ethanol was 5 to 1. The plot shows that there was good agreement with the steady state model. Similar plots were made for residence times of 30 and 45 min. with equivalent agreement. From these plots growth and nucleation rates were determined. For example, the growth rates were 0.107 mm./hr. for a 45 min. residence time and 0.272 mm./hr. for the 15 min. residence time. The intercepts yielded nuclei population densities of 8.7×10^8 and 1.95×10^9 numbers per mm. for the 45 and 15 min. residence times, respectively. Randolph and Larson (6) showed that data taken at different drawdown times could be used to determine the functional relationship between nucleation and growth. Under the assumptions previously stated with the additional assumption of constant suspension density, the following relationships obtained:

$$n_o^\circ = k_1 r^{\beta-1} \tag{8}$$

$$\frac{dN^\circ}{dt} = n_o^\circ r = k_1 r^\beta \tag{9}$$

Accordingly, a steady state plot of log nuclei population density vs. log growth rate should yield a straight line whose slope gives the kinetic order of the system under study. This plot for the alum-ethanol-water system is shown in Figure 4. Data for this plot were obtained from several steady state runs with different residence times. All of the points were from runs with an alum solution inlet concentration of 10 g./100 ml. water and with an alum solution to ethanol ratio of 5 to 1. Data were taken at residence times of 15, 30, and 45 min. The slope of this line is unity, and hence, by Equation (9), the exponent β in Equation (9) is 2. The intercept of Figure 4 is the constant k_1 in Equation (9). The relationship between growth rate and nucleation rate per liter of crystallizer volume is, therefore

$$\frac{dN^\circ}{dt} = 1.2 \times 10^9 r^2 \tag{10}$$

for the ammonium alum salting out system described.

When one uses the above equation, nucleation rates may be calculated when growth rates are known. For example, at a growth rate of 0.20 mm./hr., the nucleation rate is calculated to be 4.8×10^7 nuclei/hr./liter.

Unsteady State

In order to further test the kinetic model obtained from steady state tests, the system was operated at unsteady state. Specifically, the drawdown or residence time was changed step-by-step, and the changing size distribution was observed. To obtain this data, the system was first operated at one production rate for twenty residence times to achieve steady state; then a step change in feed rate was made to provide a different residence time.

Figure 5 shows a plot of log of population density vs. dimensionless time. The parameters for this plot are the mean crystal diameters for various size fractions. The data for this plot were taken from a run with an alum solution concentration of 10 g./100 ml. water and a 5 to 1 ratio of alum solution to ethanol. A 45 min. residence time was used to attain initial steady state. The start-up transient provides a vivid picture of the initial shower of crystals induced by the sudden supersaturation caused by mixing of the alum solution and ethanol. This shower grew its way through the size fraction and was observed as maximum points in subsequent sizes.

The cyclic nature of the curve may be explained by considering what the initial shower of nuclei did to the system. This shower was caused by sudden increase in supersaturation. The shower propagated as a wavelike disturbance. As this wave disturbance traveled along the size axis, the total area changed. This change in area altered the degree of supersaturation causing reductions in the growth and nucleation rates. The disturbances dampened out very early for the small size fractions. A period of twenty residence times was required before these start-up disturbances damped out and a steady state distribution was reached.

After initial steady state was reached, the residence time was changed to 15 min. Figure 5 shows that this

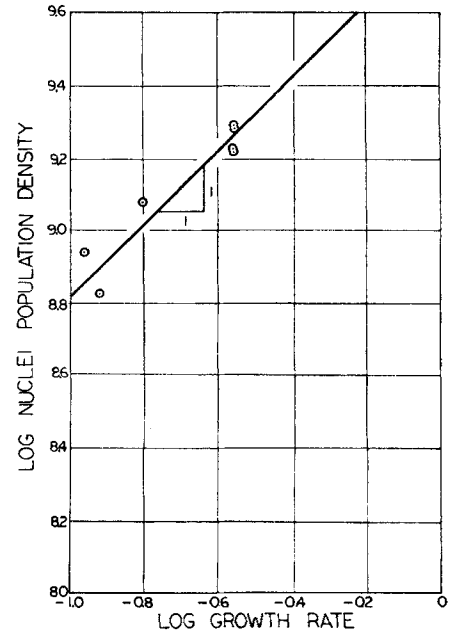

Fig. 4. Plot of log steady state nuclei population density vs. log steady state growth rate.

step change introduced a definite disturbance to the size distribution. Here again the disturbance first occurred in the small crystals and grew its way through the size fraction. A new final steady state condition was reached approximately 4.5 hr. after the change. This corresponds to eighteen 15 min. residence times or six dimensionless residence times. Although the new steady state condition had a different growth rate, the distribution of the portion of the size fraction plotted was not appreciably different from the initial distribution.

In order to compare the above experimental results with the model, the data were used to determine the time variation of the total crystal numbers, length, area, and volume as defined by Equations (4), (5), (6), (7). These quantities correspond to the moments of the population density.

The moment analysis transformation technique, as presented by Randolph and Larson (5), was used to transform Equation (2) into a form easily solvable on an analog computer. The resultant dimensionless transformed equations are as follows:

$$\frac{df_0}{d\theta} + af_0 = \left(\frac{a}{f_2}\right)^{\beta} \tag{11}$$

$$\frac{df_1}{d\theta} + af_1 = -f_0\frac{a}{f_2}$$

$$\frac{df_2}{d\theta} + af_2 = -f_1\frac{a}{f_2}$$

The f_i's are proportional to the total crystal suspension numbers, length, and area, respectively. θ_2 is dimensionless time, and a is the dimensionless reciprocal drawdown time. The exponent β is the exponent from the kinetic relationship between nucleation rate and growth rate shown in Equation (9). The forcing function for this closed set of ordinary differential equations is a. Thus, the set provides the model of the system for a residence time disturbance. A change in the quantity a represents a change in residence time. The initial conditions for this set are as follows (5):

$$f_0(0) = 1 \tag{12}$$

$$f_1(0) = -1$$

$$f_2(0) = 1$$

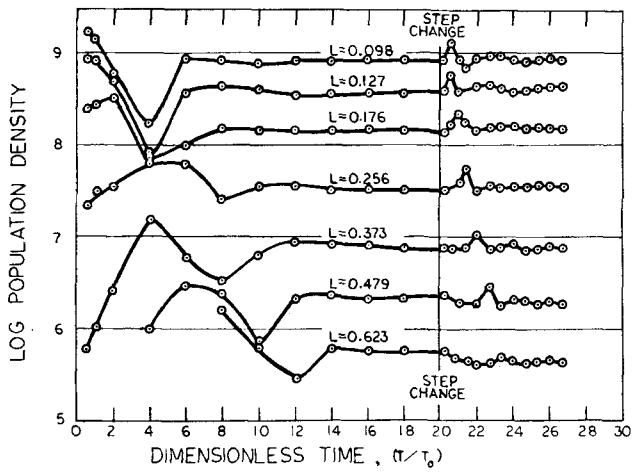

Fig. 5. Plot of log population density vs. dimensionless time for start up and production rate change: 5.5-liter vessel, 5/1 ratio of alum solution to ethanol, 10 g./100 ml. water alum solution concentration, 45-min. initial residence time, 15-min. final residence time, T_0 = 45 min.

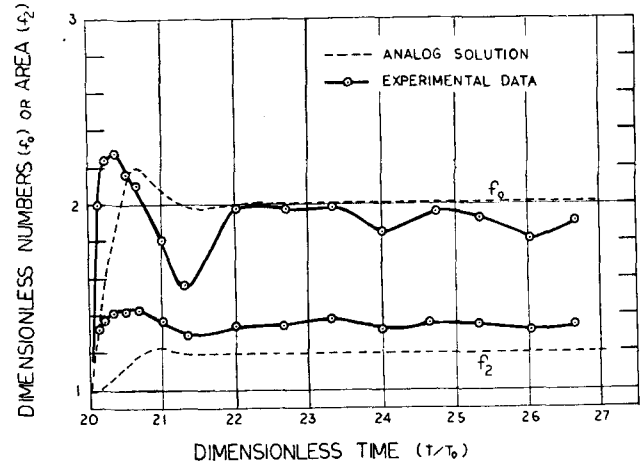

Fig. 6. Plot of experimental and second-order theoretical change in dimensionless numbers (f_0) and area (f_2) vs. dimensionless time as a result of a threefold step increase in production rate: T_0 = 45 min., T_{final} = 15 min.

Equations (11), subject to initial conditions (12), were solved on the analog computer for β equal to 2.

The experimental transient quantities for comparison with the dimensionless f_i were calculated by the following equation:

$$f_i = \frac{J_i/(J_i)_0}{(-1)^i i!} \tag{13}$$

where the J_i's were obtained from Equations (4) through (7), and $(J_i)_0$ was the initial steady state value of the respective J_i's.

The small particles could not be counted, and the ln n^0 vs. L plot was not a straight line during unsteady state operation; therefore, neither an accurate actual count of particles in the near nuclei range nor an extrapolated count was available for determination of the transient moments. In order to compare experimental data with the computer solution, an additional assumption was made in the calculation of the experimental moments. It was assumed that the transient moments were oscillations around their final steady state values. The final steady state values could easily be determined and were used to correct the measured unsteady state moments. This assumption implied that the small crystals reached their final steady state density instantaneously after the disturbance. The assumption is not greatly in error as seen in Figure 5, and because the small crystals dominate the numbers count, it does have the effect of shortening the rise time in the initial period of the transient, and it magnifies the transient in the initial period.

The analog computer soluton to Equations (11) (second-order model) along with the experimental f_i's calculated from Equation (13) are plotted on Figures 6 and 7. Figure 6 shows f_0 and f_2, and Figure 7 shows f_1 and f_3. The plots are for the transient period after the residence time was decreased by a factor of 3 (a = 3). The data are from a run where the initial and final residence times were 45 and 15 min., respectively.

As can be seen, the initial experimental rise time was much shorter than the computer initial rise time. This, as previously stated, resulted from the assumption that the small crystal population density instantaneously reaches a new steady state. These plots show, however, that there were indeed transients in the experimental data and that they were similar to those found in the theoretical computer solution.

The final values of the predicted f_i's were different from the experimental values because, although the theo-

retical change in f_3 was zero, there was a slight difference in mass as calculated from the extrapolation of the data to zero size. It was found experimentally that the mass (f_3) was constant during the experimental step change. It is felt that the difference was quite small considering the extremely large numbers obtained in measuring the experimental distribution. It should be noted that the length of the transient period of the experimental f_i's is very close to that of the computer solution. This shows that the errors introduced by the assumption made when calculating the experimental f_i's becomes less as time goes on.

Figure 8 shows a similar plot of f_o and f_1 along with the computer solution to a cubic kinetic model. It can be seen that there was little similarity between this cubic model and the data.

The conclusion that can be drawn from these dynamic plots is that the second-order model was the best one. But further than that, the transient test provides another method of estimating the kinetic order of the crystallization system under study. The steady state technique outlined by Figure 3 provides one method, but this method by itself does not have the strength that the combined dynamic and steady state methods have.

SUMMARY

This work resulted in the development of a simple system to illustrate a technique for determining quantitatively growth and nucleation rates and their relationship in continuous crystallization. This particular apparatus and crystallizing system reduced many of the operational uncertainties which tend to obscure the fundamentals of nucleation and growth. Consequently, the apparatus and technique developed could be used with excellent advantage as a laboratory experiment for teaching the fundamental relationships between crystal growth and nucleation kinetics. It could be easily adapted as a unit operations laboratory experiment.

For the system selected the growth and nucleation kinetics were determined from steady state data, and it was shown that these relationships predicted the unsteady state behavior of the process. It was shown that unsteady state behavior more clearly reflects the kinetic order of growth and nucleation than does the steady state behavior. This suggests that both must be studied to obtain a complete picture of the system. The greatest difficulty and uncertainty experienced was in the description of the distribution of the very small crystals. In terms of numbers, the very small crystals dominate the size distribution behavior. This problem will be attacked in future work by use of a counter capable of sizing and counting crystals down to the 1-μ range. This additional information should result in even better agreement between prediction and experiment than has been shown in this work.

Some of the first transient size distribution data obtained under closely defined conditions have been presented. Also presented is a method for finding quantitative relationships between growth and nucleation kinetics with only the size distribution of the crystalline product used. Data such as this can easily be obtained from a sizeable number of industrial crystallizers.

The kinetic relationships proposed are simple and admittedly empirical. However, considering the complexity of the more fundamental models proposed in the literature as well as the many factors influencing nucleation and growth, it is felt that this approach offers a fruitful source of data which may be used to improve the operation of commercial processes. In any event, if more sophisticated models for growth and nucleation are shown to be preferable, they can still be incorporated in the overall numbers balance equation with advantage.

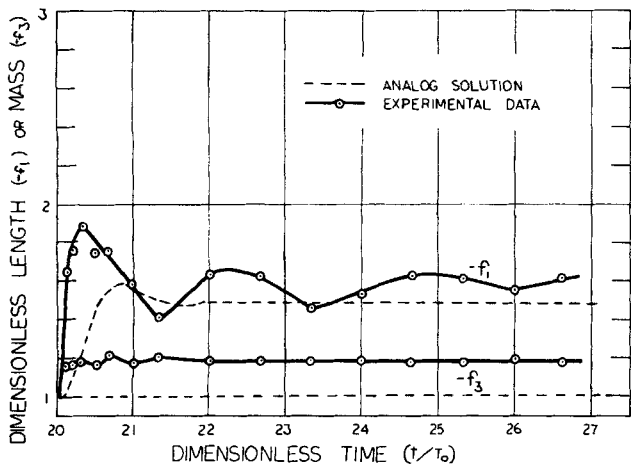

Fig. 7. Plot of experimental and second-order theoretical change in dimensionless length (f_1) and mass (f_3) vs. dimensionless time as a result of a threefold step increase in production rate: T_o = 45 min., T_{final} = 15 min.

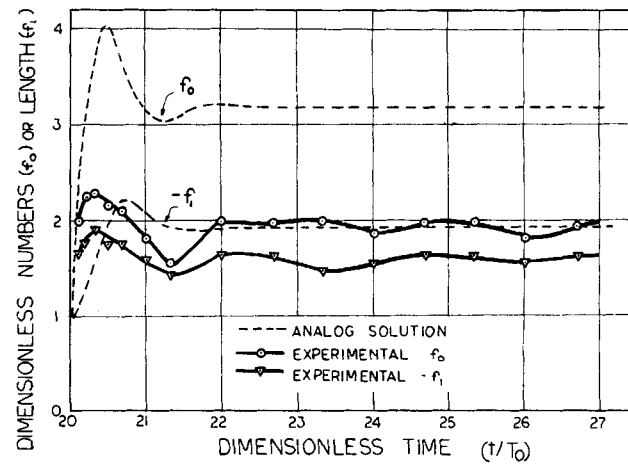

Fig. 8. Plot of experimental and third-order theoretical change in dimensionless numbers (f_o) and length (f_1) vs. dimensionless time as a result of a threefold step increase in production rate.

ACKNOWLEDGMENT

This work was supported in part by the National Science Foundation Research Grant G-2156.

NOTATION

a	=	dimensionless reciprocal residence time
A_T	=	total crystal area, sq. mm.
f_i	=	dimensionless moments of population density
J_i	=	moments of the population density
k_1	=	proportionality constant
K_a	=	area shape factor
K_v	=	volume shape factor
l	=	total length of size distribution, mm.
L	=	crystal size, mm.
L_T	=	total crystal length, mm.
$\bar{L}$	=	average crystal size, mm.
M_T	=	total crystal mass, g.
Δm	=	mass fraction, dimensionless
n	=	population density, number/mm.
n^o	=	nuclei population density, number/mm.
N_T	=	number of crystals
N^o	=	number of nuclei
r	=	linear growth rate, mm./hr.

T = residence time, hr.
t = time, hr.
V = crystallizer volume, liters
β = kinetic order
ρ = particle density, g./cu. mm.
ρ_s = suspension density, g./liter
θ = dimensionless time
sub o = steady state

LITERATURE CITED

1. Bransom, S. H., W. J. Dunning, and B. Millard, *Disc. Faraday Soc.*, **5**, 83 (1949).
2. Larson, M. A., and D. C. Murray, A laboratory study of continuous mixed suspension crystallization. Preprint 14, Fiftieth Natl. Meeting, A.I.Ch.E., Buffalo, New York (1963).
3. McCabe, W. L., *Ind. Eng. Chem.*, **21**, 112 (1929).
4. Murray, D. C., Ph.D. thesis, Iowa State Univ., Ames, Iowa (1964).
5. Randolph, A. D., and M. A. Larson, Analog simulation of dynamic behavior in a mixed crystal suspension. Preprint 38, Fifty-fifth Ann. Meeting, A.I.Ch.E., Chicago, Illinois (December 2-6, 1962).
6. ————, *A.I.Ch.E. J.*, **8**, 639 (1962).
7. Robinson, J. N., and J. E. Roberts, *Can. J. Chem. Eng.*, **35**, 105 (1957).
8. Saeman, W. C., *A.I.Ch.E. J.*, **2**, 107 (1956).

Manuscript received October 7, 1964; revision received February 23, 1965; paper accepted February 26, 1965. Paper presented at A.I.Ch.E. Boston meeting.

The Numerical Solution of Boundary-Layer Problems

D. D. FUSSELL and J. D. HELLUMS

Rice University, Houston, Texas

A new method for numerical solution of boundary-layer problems has greater applicability as well as greater speed and accuracy than the several previously proposed methods. The method uses the Goertler-transformed equations and a nonlinear finite-difference procedure. In most earlier work on difference methods the equations have been linearized at each step parallel to the boundary. The method of treatment of the boundary conditions on the equation of change for energy or mass transfer is shown to have an important influence on accuracy, and a new, more accurate method of treating boundary conditions involving the normal derivative is presented.

Typical complete solutions are compared with the several methods. The solutions include both similar and more general flows up to separation, as well as coupling between the momentum and energy-balance equations.

The boundary-layer problems of most interest today involve high temperatures, large variations in physical properties, ionization, chemical reactions, and other phenomena that greatly complicate the application of series expansions or other classical methods of solution. Interest has increased therefore in recent years in the development of numerical methods of general applicability. One such method that holds important advantages over previously proposed methods is presented here, with a number of comparisons with results from previously proposed methods. One of the interesting results of the work is that a nonlinear finite-difference procedure was finally adopted as being much more efficient and accurate than procedures of the usual type, where the difference equations are linearized at each step in the procedure.

Hartree-Womersley Methods

A well-known class of methods is based on the procedure of Hartree and Womersley (*9*), used with some success long before the advent of the modern digital computer. This method, with certain modifications, has been used and advocated by several workers (*14, 17* to *19*). The basic idea of Hartree and Womersley was to approximate the derivatives with respect to the X direction by using divided differences and to leave the derivatives in the Y direction in differential form. Hence, the procedure involved the solution of a system of ordinary differential equations at each X step as the solution was propagated in the positive X direction. The ordinary differential equations are solved by the well-known techniques for integration of initial-value problems. The method of satisfying the boundary conditions is a great disadvantage of the Hartree-Womersley methods. Conditions at the outer edge of the boundary layer are satisfied by assuming sufficient additional conditions at the boundary to make integration possible as an initial-value problem starting at the boundary. The computed values of the functions at the outer edge are then compared with the desired values, the assumed conditions are corrected, and the procedure is repeated until the outer conditions are satisfied. This technique of satisfying the boundary conditions has been found (*17, 18*) satisfactory in classical boundary-layer problems where the momentum and energy-balance equations are uncoupled, since a single condition is imposed at the outer edge. However, since two or more exterior conditions must be satisfied simultaneously, the procedure is cumbersome in problems involving a coupled energy balance and one or more diffusion relationships.

Smith and Cutter found the Hartree-Womersley method applicable only for grid spacings where ΔX was larger than $X/25$ at all grid points; for smaller values of ΔX the solutions diverged, giving clear evidence of instability. The method cannot be considered generally applicable because of the stability problem, even though it gave reliable results in several applications. (*17, 18, 19*).

Finite Difference Methods

The second class of methods includes all those that might be designated *finite-difference methods*. All derivatives are approximated by divided differences. The solution is propagated in the positive X direction by solving the resulting system of algebraic equations at each X step. Hence, the boundary conditions are satisfied in the basic algebraic procedure. Of the many possible difference methods, prior workers on nonlinear differential equations have almost invariably selected those in which the difference equations are made linear at each step in the procedure. Such a selection, which greatly simplifies the algebraic procedure, has been found satisfactory in many cases.